Chemical Science

Accepted Manuscript

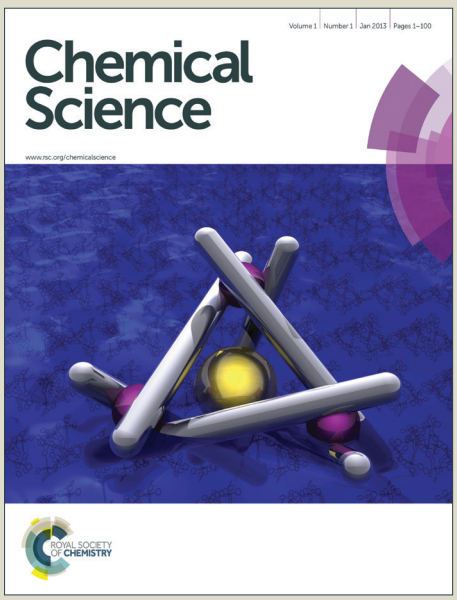

ROYAL SOCIETY OF CHEMISTRY

www.rsc.org/chemicalscience

Research Article

Computational discovery and experimental verification of tyrosine kinase inhibitor pazopanib for the reverse of memory and cognitive deficits in rat model of neurodegeneration

Yongliang Yang[1*], Guohui Li[2*], Dongyu Zhao[1], Haoyang Yu[3], Xiliang Zheng[4], Xiangda Peng[2], Xiaoe Zhang[1], Ting Fu[2], Xiaoqing Hu[1], Mingshan Niu[1], Xuefei Ji[3], Libo Zou[3*], Jin Wang[4,5*]

[1]Center for Molecular Medicine, School of Life Science and Biotechnology, Dalian University of Technology, Dalian, 116023, P.R.China;

[2]Laboratory of Molecular Modeling and Design, State key Laboratory of Molecular Reaction Dynamics, Dalian Institute of Chemical Physics, Chinese Academy of Sciences, 457 Zhongshan Rd. Dalian 116023, P.R.China;

[3]Department of Life Science and Biopharmaceutics, Shenyang Pharmaceutical University, Shenyang 110016, P.R.China;

[4]State Key Laboratory of Electroanalytical Chemistry, Changchun Institute of Applied Chemistry, Chinese Academy of Sciences, Changchun, Jilin, China;

[5]Department of Chemistry and Physics, State University of New York, Stony Brook, New York, USA;

*Corresponding authors: **Yongliang Yang**, E-mail: everbright99@foxmail.com; **Guohui Li,** E-mail: ghli@dicp.ac.cn; **Libo Zou,** E-mail: libozou@163.com; **Jin Wang**, E-mail: jin.wang.1@stonybrook.edu

Running title: pazopanib rescues memory and cognitive deficits

Abstract

Cognition and memory impairment are hallmarks from the pathological cascade of various neurodegenerative disorders. Herein, we developed a novel computational strategy with a two-dimensional virtual screening for not only affinity but also specificity. We integrated two-dimensional virtual screening with ligand screening of 3D shape, electrostatic similarity and local binding site similarity to find existing drugs that may reduce the signs of cognitive deficits. For the first time, we found that pazopanib, a tyrosine kinase inhibitor marketed for cancer treatment, inhibits acetylcholinesterase (AchE) activities at sub-micromolar concentration. We evaluated and compared the effects of intragastric administered pazopanib with donepezil, a marketed AchE inhibitor, in cognitive and behavioral assays including the novel object recognition test, Y maze and Morris water maze test. Surprisingly, we found that pazopanib can restore memory loss and cognitive dysfunction to a similar extent as donepezil in a dosage of 15mg/kg, only one fifth of the equivalent clinical dosage

for cancer treatment. Furthermore, we demonstrated that pazopanib dramatically enhances the hippocampal Ach levels and increases the expression of the synaptic marker SYP. These findings suggest that pazopanib may become a viable treatment option for memory and cognitive deficits with a good safety profile in human.

Significance Statement

In the present work, we developed a novel computational strategy with a two-dimensional virtual screening for not only affinity but also specificity. We integrated the two-dimensional virtual screening with ligand screening of 3D shape, electrostatic similarity and local binding site similarity to find existing drugs that may reduce the signs of cognitive deficits. For the first time, we found that pazopanib, a tyrosine kinase inhibitor (TKI) marketed for cancer treatment, abrogates the course of neurodegeneration.

Introduction

With the increase of aging population worldwide, neurodegenerative disorders such as Alzheimer disease (AD)(1), Parkinson disease (PD)(2) and Huntington disease (HD)(3) remain to be devastating diseases for which effective treatment are urgently needed. Memory dysfunction and cognition impairment are the most common symptoms affecting patients with neurodegenerative diseases(4). To date, only four approved small molecule therapeutics are on the market of which three are acetylcholinesterase (AchE) inhibitors (donepezil, rivastigmine and galanthamine) for the treatment of mild to moderate AD symptoms(5). Unfortunately, there are no

definitive evidences yet showing the use of donepezil or other agents can alter the course of AD progression. Hence, the search is still on for molecules with tolerable side effects to benefit older patients with neurodegenerative disorders.

Traditionally, binding affinity has been used as the criterion in the virtual screening process for drug discovery. Yet, binding specificity is also crucial in the practice of drug design and discovery(6). We developed a novel way to quantify specificity (7, 8) based on our energy landscape theory of ligand binding (9, 10). The native binding mode and the non-native conformations during the binding between a ligand and a receptor are statistically distributed in energy. Herein, specificity is quantified by ISR (Intrinsic Specificity Ratio) value, calculated as $\frac{\delta E}{\Delta E\sqrt{2S}}$, where δE is the energy gap between the native binding mode and the average non-native binding states, △E is the energy variance or spread of the non-native states and S is the configurational entropy measuring the size of the configurational space which scales with the size of the system (number of atoms). In other words, the entropy S represents the configurational entropy measuring the size of the configurational space that scales with the size of the system (number of atoms), which is the ligand-receptor binding complex in our study.

. In the current study, the receptor targets are fixed as rigid, the ligands are flexible with certain flexible torsional bonds, the entropy S depends approximately linearly on the number of torsional bonds of each ligand molecule with the constant coefficient on the order of 1. The S is only relevant to the size of the system, which is constant during the binding process for a specific ligand binding to the receptor. Consequently, a large ISR value leads to a high level of discrimination of the native binding mode from the non-native binding modes, which implies high intrinsic

specificity (9, 10). One can imagine a large receptor as composed of small receptors connected together through linkers. Then the explorations on the structures (binding modes) for the same (large) target and explorations on the sequences for different (small) receptors for the same ligand are approximately equivalent (7, 8). Therefore, the intrinsic specificity is expected to be correlated with the conventional specificity of discriminating of affinities among different receptors for the same ligand (7, 8) for large receptors. In this way, one can quantify the intrinsic specificity only with the specific target and infer the conventional specificity without the need for searching through all the receptor universe. The two dimensional virtual screening strategy with not only affinity but also specificity can be used to search for drug candidates such as inhibitors of COX-2(7, 8), human serum albumin (HSA) (11) and Ras protein(12) etc.

In this work, we first employed the two dimensional virtual screening strategy for 1385 FDA-approved small molecule drugs with AchE as the receptor structure. Interestingly, three tyrosine kinase inhibitors (TKIs), Sorafenib, Pazopanib and Sunitinib stand out as three top hits. Meanwhile, we used ligand-based virtual screening with donepezil as the query molecule to search against the 1385 FDA-approved small molecule drugs retrieved from the DrugBank database(13). The ligand virtual screening was performed by the ROCS program with similar three dimensional shapes(14) and the EON program with electrostatics(15). Consistent with the results from the above two dimensional virtual screenings, three TKIs (Sorafenib, Pazopanib and Sunitinib) are also among the top 50 hits of ligand virtual screening. In

addition, we employed a local binding site similarity screening(16, 17) with AchE as the query structure to search against a set of 1105 crystallographic structures of 377 approved drug targets retrieved from the Drugbank. Intriguingly, the majority of top-ranked targets belong to protein kinases. Remarkably, consistent with the computational prediction, we found that pazopanib inhibits AchE with sub-micromolar affinity. We explored pazopanib for its ability to rescue memory dysfunction and cognitive deficits in a rat model induced by quinolinic acid (QA)(18). For the first time, we found that pazopanib is able to restore memory and cognitive deficits to a similar extent as with donepezil in dosage of just 15mg/kg.

Results

Two dimensional drug screening with both affinity and specificity against AchE

The two dimensional virtual screening of 1385 FDA-approved small molecule drugs (http://www.drugbank.ca/) against AchE was performed by AutoDock 4.20 program (see Figure 1). The binding affinity and ISR value for each molecule were recorded and used for the ranking. The 1385 approved drugs were used for making the contour map of two dimensional drug screening (Figure 2b). Donepezil has high values in both affinity (12.24 kcal/mol) and intrinsic specificity (ISR=3.31) among all the approved drugs. Three TKIs, sorafenib (affinity: -10.41 kcal/mol; ISR: 3.00), pazopanib (affinity: -11.80 kcal/mol; ISR: 2.61) and sunitinib (affinity: -9.74 kcal/mol; ISR: 2.26) are the other three top hits considering both affinity and the ISR value.

Ligand virtual screening with 3D shape and electrostatic comparison

The three dimensional shape comparison between donepezil and 1385 FDA-approved drugs (http://www.drugbank.ca/) was performed by the ROCS program implemented within OpenEye (Rapid Overlay of Chemical Structures, version 3.1, OpenEye Scientific Software). The unique feature of ROCS is that it ranks compounds by their shape Tanimoto score, a quantitative assessment of three-dimensional overlap with a range from 0-1 (1 represents complete overlap). The molecule shape is computed by atom-centered overlapping Gaussian functions and the shape Tanimoto score is calculated by the maximal intersection of the volume of two molecules. The top 50 'hits' had Tanimoto scores between 0.65 and 0.83. Next, we re-ranked the ROCS hits for electrostatic similarity with donepezil by the program EON (version, 3.1, OpenEye, Scientific Software), which computes the electrostatic Tanimoto score ranging from one (identical) to negative values judging by the overlap results of positive and negative charges. The electrostatic Tanimotos for the ROCS hits in the EON comparison ranged from -0.51 to 0.65. The final top 50 hits were re-ranked by the score of EON_ET_Combo, which is the sum of 3D similarity and electrostatics similarity. The results were then manually inspected. Nearly one third of the top 50 hits belong to antipsychotic and antidepressant drugs (17 out of 50, see Supplementary Table 3). For practical reasons, they were ruled out for further experimental testing. Interestingly, sorafenib, pazopanib and sunitinib, three tyrosine kinase inhibitors (TKIs), are among the top 50 hits (see Supplementary Table 3). Pazopanib and donepezil were superimposed and displayed by VIDA program

(version 3.1, OpenEye Scientific Software) with the shape Tanimoto value of 0.612 and electrostatic Tanimoto score of 0.675 (Figure 2d).

Local binding site similarity of AchE with approved drug targets

The searching of local binding site similarity among multiple targets is essential for studying polypharmacology(19). We compiled 377 FDA-approved drug targets from the DrugBank which led us to retrieve 1105 crystallographic structures from the PDB bank. Next, we searched and compared the pairwise ligand binding site similarity between AchE and the 1105 protein targets by TM-align(20), a structure alignment and comparison tool recommended in the PDB bank (http://www.pdb.org). Interestingly, 14 out of the top 20 ranked targets by local binding site similarity belong to the protein kinase family and the majority belongs to tyrosine kinase including VEGFR2, EGFR, Src, JAK1, ERBB4, ERBB2, Lyn, JAK2, FGFR2, MAPK2 and HCK (see Supplementary Table 1 and 2). The remaining protein targets belong to carboxylesterase, opioid receptor and phospholipase families etc. The pairwise similarity TM-score between the pocket of VEGFR2 and AchE is about ~0.31 (TM-score>0.30 suggests the significance, see Figure 2c, Supplementary Table 1 and 2).

AchE enzymatic assay screening

The AchE enzymatic assay screening experiments determined that pazopanib is the most potent molecule among thirteen TKIs with IC_{50} value of 0.93 μM (see Figure 2d). The IC_{50} value of sunitinib is 5.87 μM. Sorafenib as well as other TKIs are weak

binders for AchE (IC_{50} > 10μM, see Supplementary Table 4 for details).

Pazopanib binds with AchE similarly to donepezil

We performed molecular docking combined with molecular dynamics (MD) simulations to assess the possible binding mode of pazopanib with AchE. In short, the MD simulations (three independent 300ns simulation and one independent 1000ns simulation) revealed that pazopanib can fit well into the pocket of AchE (see Figure 3). Similar with donepezil, pazopanib makes putative hydrophobic contacts with Tyr^{279}, Tyr^{121}, Trp^{84}, and $Phe^{330-331}$. Moreover, analogous to donepezil, it seems that pazopanib does not interact directly with the catalytic triad of AchE(21) (Ser^{200}, Glu^{327} and His^{440}, see Figure 3b). These results suggest that pazopanib binds with AchE similarly to donepezil.

Effects of pazopanib on the cognition impairment of rat model in the novel object recognition test

To assess whether pazopanib can restore cognition deficits, we used the novel object recognition test(22) as a behavioral assay to evaluate the recognition memory. Compared to the control group, the model group showed significant impairment on the novel object exploration/recognition. On the other hand, both the treatment group with donepezil and pazopanib improved the performance on the novel object recognition test (see Figure 4a and 4b). The treatment group with pazopanib in high dose (15mg/kg) returned this phenotype to a similar extent as the treatment group with donepezil (0.95mg/kg).

Effects of pazopanib on the memory dysfunction in the Y maze cognitive behavioral assay

The Y maze cognitive behavioral assay(23) is conducted to measure the short-term working memory for model rats treated with pazopanib and donepezil. A significant lower spontaneous alternation response rate was observed for the model group compared to the control group injected with PBS solution. In contrast, the treatment group with pazopanib restored this phenotype to a similar extent as the treatment group with donepezil (Figure 4c and 4d). These data indicate that pazopanib can improve the short-term working memory of animals in a similar manner to donepezil.

Effect of pazopanib on the spatial memory impairment in the Morris water maze

The Morris water maze (MWM) task demands incremental learning of a fixed platform location throughout the training period which results in the formation of spatial reference memory(24). Compared to the control-group rats (control group), we observed that the model group spent significantly more time and distance in finding the hidden platform. On the other hand, when donepezil (0.95mg/kg) was administered by intragastric infusion, the model rats showed a significant decrease in time and distance to find the hidden platform. Interestingly, when pazopanib was administered to the model rats, they showed a similar decrease in time and distance to find the hidden platform in a dose dependent manner (see Figure 5a-b). Subsequently, we performed probe trials experiments in which the platform was removed. The model rats with spatial memory deficits were unable to develop a spatial preference

for the area around the platform. By contrast, the control group as well as the model group administered with donepezil or pazopanib demonstrated a clear spatial preference in the correct quadrant of the platform (Figure 5c-d). Moreover, bivariate histograms of the swimming patterns revealed that the treatment group with pazopanib (15mg/kg) also developed a spatial preference in the correct quadrant of the removed platform (Figure 5d). Together, the above results suggest that pazopanib can reverse the spatial memory deficits in a fashion similar to donepezil.

Pazopanib enhances hippocampal Ach levels in the model rats

We used ELISA assay to detect acetylcholine (ACh) levels in the hippocampus of control and drug-treated rat group. In agreement with prior findings (25), the QA-induced rats demonstrate a significant reduction of hippocampal Ach release as compared to the control group. Remarkably, pazopanib administration was able to prevent the QA-induced decrease of ACh level in a dose dependent manner (see Figure 6a). The beneficial effect of 15mg/kg pazopanib was similar in extent to the donepezil-treated group. This demonstrates that pazopanib prevents the cholinergic degeneration and enhances Ach levels in the model rats.

Pazopanib increases the expression of synaptic markers in the model rats

Synaptophysin (SYP) is a synaptic vesicle protein and has been widely used as a presynaptic marker for pre-synaptic terminals(26). The expression level of SYP is significantly correlated with cognitive degeneration and the progression of neurodegenerative diseases(27, 28). We observed a decrease of SYP level in the CA1

region of the model group compared with the control group by western blotting, whereas SYP expression level was increased in donepezil- and pazopanib-treated model rats (Figure 6b and 6c). In addition, PSD-95 is also a synaptic marker and plays an important role in synaptic maturation and pathogenesis of neurodegenerative disorders(29). The effects of donepezil and pazopanib on PSD-95 level in the hippocampus and the cerebral cortex of treated animals are not statistically significant compared to the control group. Nevertheless, we observe a trend towards the decrease of PSD-95 level in the model group and a trend towards the increase of PSD-95 level in donepezil- and pazopanib-treated group (see Supplementary Figure 2). These data suggest that pazopanib might be able to protect the synapses and prevent the progression of neurodegenerative diseases.

Discussion

There are still unmet needs for disease-modifying therapies of neurodegenerative disorders with convenient dosing and excellent safety profile. The identification of approved drugs for new uses becomes an attractive strategy as a complement to conventional approaches. The established safety profile for existing drugs might substantially reduce the time and cost to advance candidate compounds into the clinical trials(30). Recently, minocycline, a tetracycline antibiotic to treat the bacterial infection has been found to reduce the level of pro-inflammatory mediators and microglial activation in AD mouse model(31). However, of note, the beneficial dosage of minocycline (40-50 mg/kg/day) in AD animals is about 1.25-1.45 fold

higher than the recommended maximum clinical dose for the treatment of bacterial infection. More recently, Cramer et al have found that the drug bexarotene which is FDA-approved for the treatment of cutaneous T cell lymphoma can rapidly reverse memory deficits in AD mouse model(32). However, the effective dosage of bexarotene used in AD animal models was 3-fold higher than that used in clinical cancer treatment. Therefore, it is of priority to find candidate compounds to treat AD and other neurodegenerative disease with acceptable dosage and tolerability for older patients.

In light of this, we designed a computational strategy of coupling two dimensional virtual screening, ligand-based screening with 3D-shape and electrostatic similarity, and local binding site similarity comparison to search approved drugs for the treatment of AD and other neurological disorders (see Figure 1). The intrinsic specificity ratio (ISR) for discrimination based on energy landscape theory of ligand binding(7) has been demonstrated to be well correlated with the structural fit or structural specificity. Therefore, the concept of two-dimensional screening has the advantages of considering both affinity and specificity, the two requirements for efficient biomolecular recognition (33, 34). The ligand shape and electrostatic similarity-comparison is based on the rationale that two similar ligands in volume and physical-chemical properties are likely to have similar target-binding activities. For instance, this approach has been found quite useful by Churchill et al (35) in the identification of the first small molecular inhibitor of NAADP (nicotinic acid adenine

dinucleotide phosphate). On the other hand, the local binding site similarity-comparison is based on the hypothesis that similar binding sites most likely bind the same molecules. This approach has led to a few successful reports(36) such as the identification of HIV-protease inhibitor Nelfinavir as anti-cancer agent(37) and the identification of the PD drug Comtan for the treatment of Tuberculosis(38). The ligand 3D shape and electrostatic-similarity comparison of donepezil with 1385 approved drugs has indicated that three TKIs (sunitinib, pazopanib and sorafenib, see Supplementary Table 3) are among the top 50 hits. We compared the binding pocket of AchE with the 1105 ligand binding sites of approved drug targets by a pairwise structure alignment and a similarity-comparison tool. The local binding site similarity comparison study has concluded that the majority of the top-ranked hits (70%, 14 out of top 20, see Supplementary Table 1 and 2) belong to protein kinases among which 8 hits are protein tyrosine kinases (PTK). We chose and purchased TKIs for further experimental testing for two practical reasons: 1. TKIs are among the top hits in our integrated computational pipelines; 2. TKIs are structurally divergent molecules with easy accessibility. We identified pazopanib as the most potent molecule with sub-micromolar affinity among the 13 purchased TKIs by enzymatic assay (see Supplementary Table 4). Of note, this is the first report of integrating two-dimensional virtual screening, ligand-based screening and local binding site similarity-comparison to narrow down the list of candidate molecules for further experimental testing.

Our results suggest that pazopanib restored memory loss and cognition impairment in a rat model induced by quinolinic acid (QA). We found that pazopanib improves learning and memory deficits in a dose-dependent manner through *in vivo* experimental settings. Particularly, pazopanib treatment at a dosage of 15mg/kg prevented the QA-induced neurodegeneration to a similar extent as donepezil at a dosage of 0.95mg/kg for rats, equivalent to the maximum dosage of 10mg/day for human. This is significant because our findings demonstrated that pazopanib restored the cognition and memory deficits at only one fifth of the equivalent dosage used for the treatment of carcinoma (the recommended clinical dosage of pazopanib is 800mg/daily for cancer treatment (39)). Hence, the risk of side effects for pazopanib in the treatment of neurodegenerative diseases might be minimal, given its well-tolerated safety profile in cancer treatment.

In the present study, we demonstrated the efficacy of pazopanib using QA-induced animal model because it has been well established that QA leads acutely to the loss of cholinergic neurons and therefore reproduces the neuroinflammatory events in diseases including AD, PD and HD(40, 41). Moreover, the QA-induced animal model has been widely used to resemble common pathological features of neurodegenerative disorders(42, 43). However, given that the exact pathways or pathologies of neurodegenerative disease are not definitely identified and continue to be a source of debate, one single animal model is insufficient to determine the effects of pazopanib for neurodegenerative disorders. Therefore, further studies in various

316 animal models(44) are warranted to assess pazopanib as an effective therapeutics for
317 neurodegeneration.

318 In summary, by integrating methods of two-dimensional screening, ligand-based
319 virtual screening, computational modeling, *in vitro* and *in vivo* experimental testing,
320 we predicted and found that pazopanib is a sub-micromolar affinity ligand of AchE
321 and is capable of ameliorating memory and cognitive dysfunction that characterize
322 neurodegenerative disorders. Noteworthy, pazopanib showed a similar extent of
323 activities as donepezil at a much lower dosage than that used to treat cancer. Another
324 significance of the present work is that we provide a useful paradigm for evaluating
325 new uses for approved drugs. Particularly, the concept of virtual screening based on
326 both affinity and specificity could be generally applied in drug discovery pipeline.
327 Neurodegeneration is a form of multifactorial disease and a variety of mechanisms
328 may contribute to its pathogenesis. Further studies are warranted to clarify the detailed
329 mechanism and the impact of pazopanib for the treatment of neurodegeneration. To
330 the best of our knowledge, this is the first report on the effect of pazopanib abrogating
331 memory and cognitive deficits under *in vivo* conditions.

332 **Materials and Methods**

333 **Two dimensional screening of approved drugs**

334 The Autodock 4.20 program was used to perform the two-dimensional screening of
335 approved small molecule drugs against AchE. For each molecule, we calculated the
336 binding affinity, the energy gap between the lowest binding energy state and average

binding energy, the variance of the free energies of different binding modes. The configurational entropy is also calculated which measures the size of the configurational space which scales with the size of the system (number of atoms). ISR value is calculated as $\frac{\delta E}{\Delta E\sqrt{2S}}$.

Ligand virtual screening by shape and electrostatics

We used OMEGA 2.4.6 to generate 100 conformers for each molecule of 1385 approved drugs. The input donepezil structure was entered as a query molecule for the initial screen. We used ROCS (3.1.2) for 3-dimensional shape comparisons and the top 500 hits were outputted in the order of shape Tanimoto values. For electrostatic properties comparisons (EON 2.10), the lowest-energy conformer of donepezil was used for all comparisons to re-rank the top 500 ROCS hits in the order of electrostatic Tanimoto scores. Lastly, the top 50 hits were ranked as EON_combo, the sum of 3D shape Tanimoto score and electrostatic Tanimoto score (Supplementary Table 3).

Local binding site similarity search

The crystallographic structure of AchE complexed with donepezil has been solved (PDB ID: 1EVE). 1105 protein target structures co-crystallized with ligands from the PDB bank (http://www.pdb.org/) were compiled for use. Herein, ligand binding pocket was defined as residues within 8Å of the complexed ligand and the ligand binding pockets of the 1200 protein targets were extracted by Pymol program (Educational version 1.3). Amino acid residues within 8Å of the co-crystallized ligand were defined as ligand binding pocket. TM-align program was then used to compute

the pairwise ligand binding site similarity between human AchE and 1105 protein targets. The alignment results were ranked in descending order (see Supplementary Table 1 and 2).

Animals used in the experiments

The experiments were performed strictly following the ethics regulation and institutional guidelines of university. The Sprague-Dawley (SD) rats were maintained at 21°C in standard ventilated cages holding 3 rats per cage and water ad libitum.

Rodent model of neurodegeneration induced by quinolinic acid (QA)

The injection of 2μl PBS solution (pH 7.4) containing 120nmol quinolinic acid (QA; Sigma, Shanghai) was applied to both left and right NBM of the animals following the standard protocol. The control group animals received an injection of 2μl of the vehicle PBS solution.

Drug treatment of the experimental animals

For treating experimental rats, donepezil and pazopanib (as salt) were dissolved in physiological saline containing 0.5% Tween-80. Experimental rats received daily dose of drugs or vehicle by intragastric administration until the end of experiments. For behavioral assay, drug treatments were conducted after the last trial of every day during the testing period.

Novel object recognition task

The object recognition task was performed in an open circle arena (80cm*80cm). After habituation, two identical objects (A1, A2) were placed in the arena with an

equal distance to the edge. Subsequently, the rats were exposed to the familiar open arena and allowed to explore for 5 min. The time that rats spent exploring each object (t_{A1}, t_{A2}) was recorded. After one hour, one object was replaced with a new object (B) and the time spent exploring each object (t_{A1}, t_B) was recorded. Similarly, after 24 hours, object B was replaced with another new object C and the time spent exploring each object (t_{A1}, t_C) was recorded. The object preferential index and object discrimination index were used to evaluate the performance of object recognition and calculated as: 1. preferential index(1h) = $t_B/(t_{A1}+t_B)$; 2. preferential index(24h) = $t_C/(t_{A1}+t_C)$; 3. discrimination index(1h) = $(t_B-t_{A1})/(t_{A1}+t_B)$; 4. discrimination index(24h) = $(t_C-t_{A1})/(t_C+t_B)$.

Y maze cognitive behavioral assay

During the experiments, each rat was first placed at one end of the arm and the total number (N) and the order of the arm entries were recorded by video camera for every 8 minutes. Successful spontaneous alternations are defined as consecutive triple entries of different arms choices. The spontaneous alternation response rate is calculated as: spontaneous alternation rate (%) = number of successful alternation / (N-2)*100.

Morris water maze task and probe trial test

In brief, the water maze consisted of a dark gray pool filled with opaque water. The testing platform was hidden below the opaque water surface but accessible for the rats. The animals were subjected to two trials per day for 4 days with a video system

monitoring and recording the percentage of time spent in the various quadrants. On the next day, the platform was removed and each rat was allowed to explore in the water pool for 90 s. The swimming time and the swimming distance in the quadrant where the platform was located were calculated.

Tissue handling and western blotting

Upon anesthesia, the animals were perfused transcardially with ice-cold saline solution and then paraformaldehyde solution (pH 7.4, 3.5% in phosphate buffer). Brain was immediately isolated and postfixed in 4% paraformaldehyde–2% glutaraldehyde for 48 hours at 4°C before processing for immunohistochemical analysis. Animals for western blotting analysis were dissected rapidly. Proteins (SYP and PSD-95) were detected using horseradish peroxidase-conjugated secondary antibodies (Santa Cruz Biotechnology and Abcam, USA).

Determination of Ach levels

The remaining half of 10% (w/v) homogenate (without SDS) from the immunohistochemical analysis was centrifuged for 30 min at 4°C without adding any detergent. Supernatants containing Ach were collected for assays. Brain extracts (soluble protein from PBS and insoluble protein from formic acid) from the animals were used for two-site ELISAs that specifically detect the Ach levels as suggested by the manufacturer (Shanghai HoraBio).

Molecular dynamics simulation

The starting structure of MD simulation was obtained from the best binding mode of docking. One 1000 ns and three 300 ns production molecular dynamics simulations were performed using PMEMD.CUDA enabled NVIDIA graphics processing units (GPUs) implemented with Amber 10.

Statistical analysis

Student's t-test and one-way and two-way analysis of variance (ANOVA) with Dunnett's post-test were performed using GraphPad Prism version 5.00 for Windows in statistical analysis. $P<0.05$ was considered significant.

Acknowledgments

Y. Yang laboratory thanks the support from the Research Funds for Key Laboratory of Liaoning Educational Council (Grant: L2013025) and National Science Foundation in China, Medical Board Oncology Department. X.Z. thanks National Natural Science Foundation of China (Grant no. 21190040, 11174105, 91227114, 91430217) for financial support. J.W. thanks NSF for support. G. Li thanks the support from 973 project: (grant: 2012CB721000), 863 project (grant: 2012AA01A305) and NSFC project (grant: 31070641). Y. Yang wishes to thank Prof. S. James Adelstein from Harvard Medical School for his support all along and his critical reading and comments on the manuscript.

Competing financial interest statement: The authors have declared that no competing financial interests exist.

Figures and Figure Legends

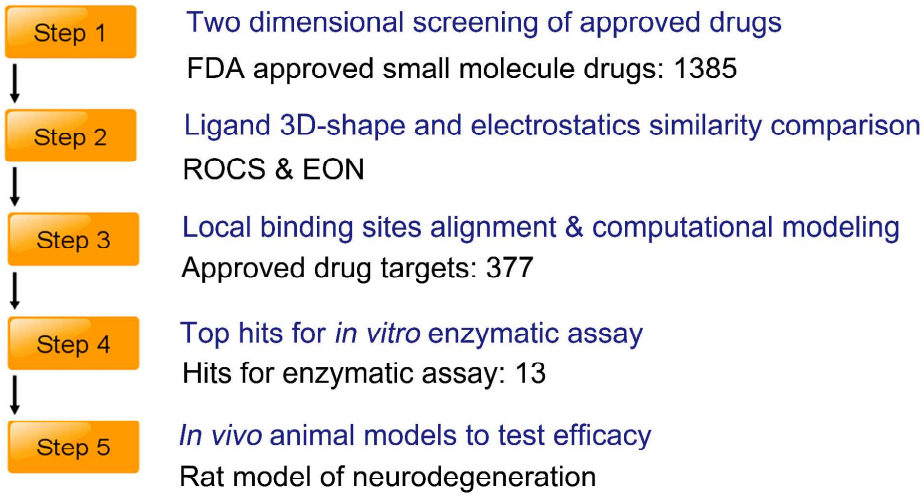

Figure 1. Discovery process of pazopanib for the rescue of neurodegeneration

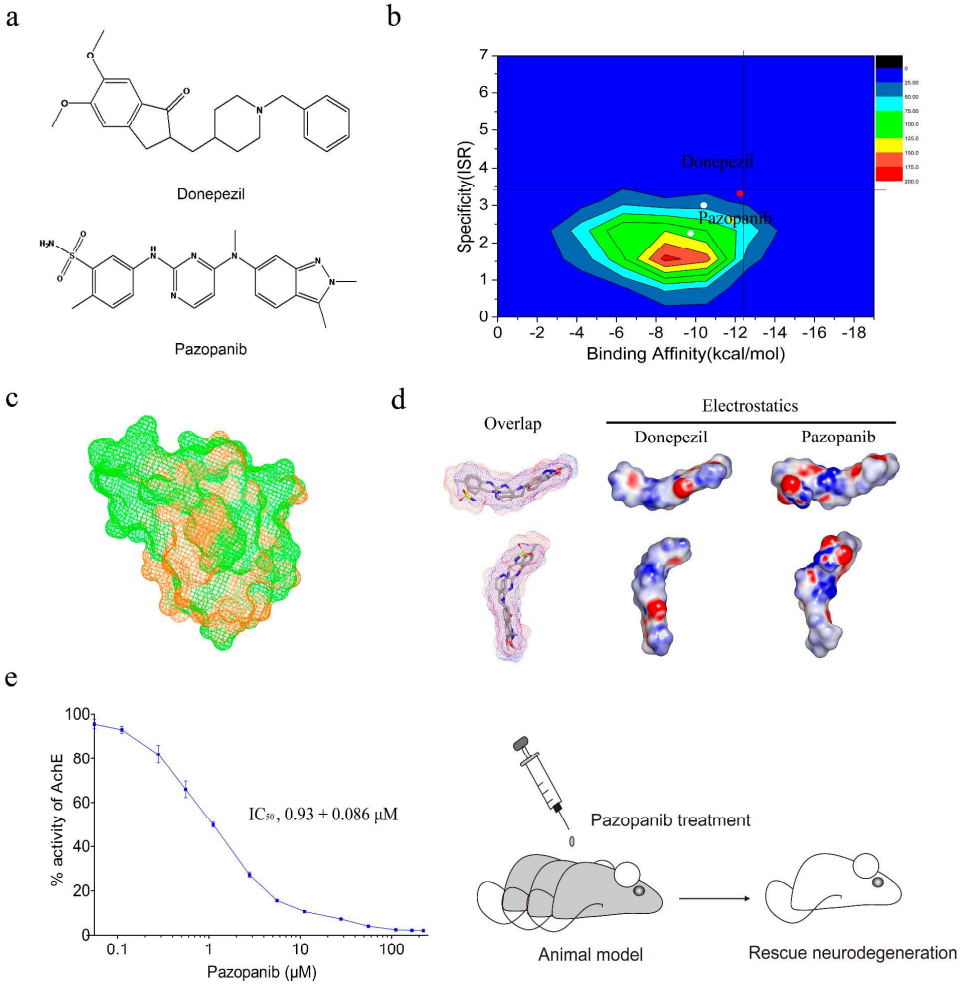

454

455 **Figure 2. Identification of pazopanib as a potent ligand of AchE.** (a)
456 Two-dimensional chemical structures of marketed drug donepezil and pazopanib; (b)
457 The contour map of affinity and ISR value for 1385 approved drugs. Donepezil is
458 depicted in red dot and pazopanib is depicted in yellow dot. Sorafenib and sunitinib
459 are depicted in white dots. The vertical axis represents ISR value and the horizontal
460 axis represents binding affinity; (c) Local binding site alignment of VEGFR2
461 (Vascular endothelial growth factor receptor 2, PDB ID: 3CJG, drug: pazopanib)

versus AchE (PDB ID: 1EVE, drug: donepezil) by TM-align program. VEGFR2 is depicted in green mesh and AchE is depicted in orange mesh. The alignment TM-score is 0.31; (d) Overlay and three-dimensional chemical structures of donepezil and pazopanib with electrostatic surfaces coded by color (red for negative charges and blue for positive charges); (e) *in vitro* AchE enzymatic assay and *in vivo* animal model test. IC_{50} value of pazopanib: 0.93±0.086μM. Animal model shows that pazopanib can rescue neurodegeneration.

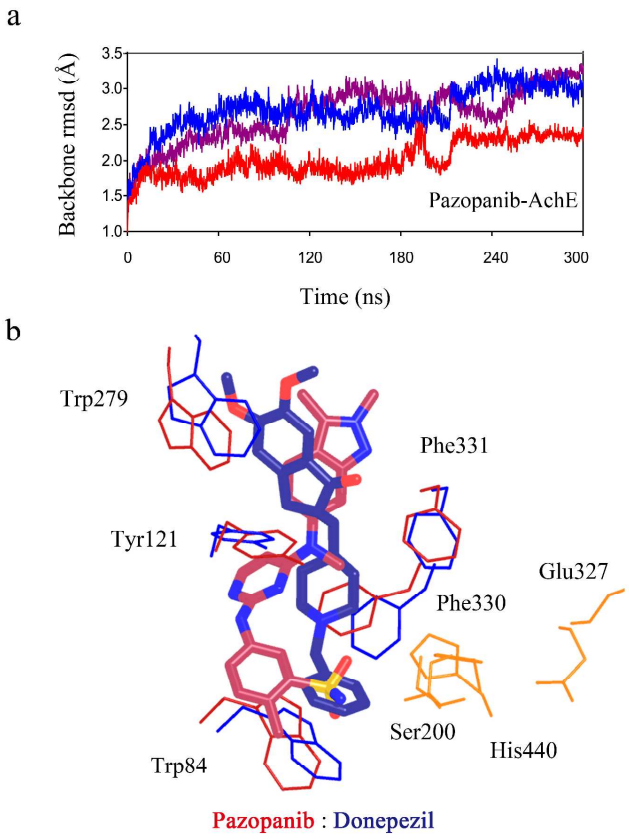

Figure 3. Computational modeling of pazopanib complexed with AchE. (a) Three independent long timescale (300ns) molecular dynamics simulation of pazopanib with AchE; (b) Overlay of complexed structure of pazopanib with AchE and

co-crystallized structure of donepezil with AchE (PDB ID: 1EVE). Pazopanib was depicted in red stick model and donepezil was depicted in blue stick model. The key residues in the catalytic pocket of pazopanib complexed with AchE were depicted in red lines and the key residues for the co-crystallized structure of donepezil with AchE were depicted in blue lines. The catalytic triad of AchE was depicted in orange lines.

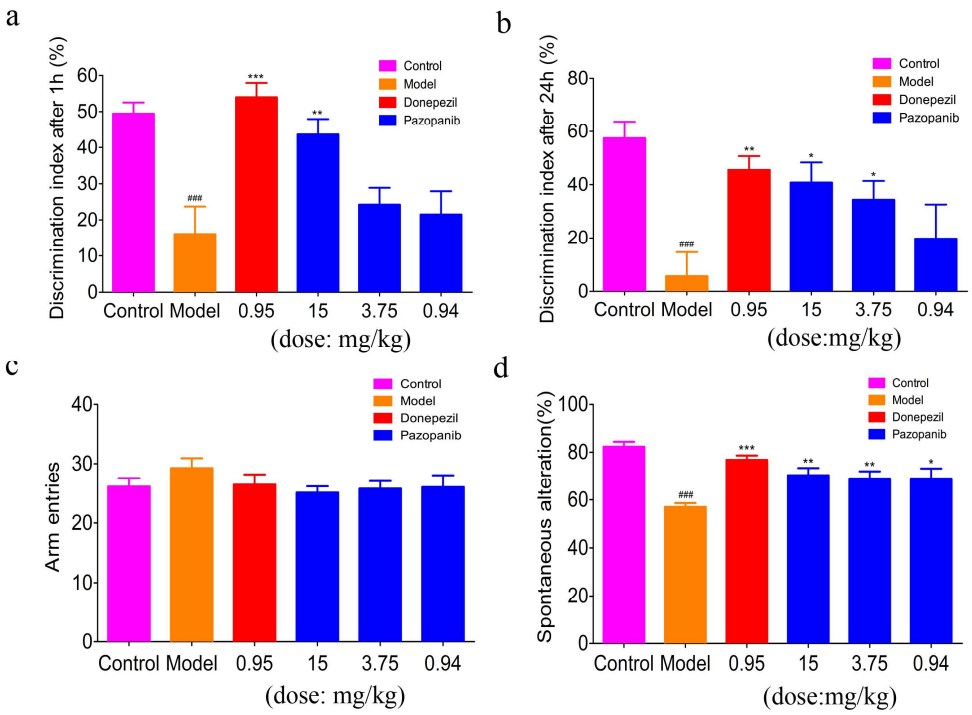

Figure 4. Effect of pazopanib on memory and cognition impairment in the novel object test and Y-maze test. (a) The discrimination index for the novel object at 1h in test session; (b) The discrimination index for the novel object at 24h in test session. Results were expressed as mean ± SEM (n=10-12) and analyzed with one-way ANOVA, followed by Dunnett's post test for multiple comparisons. ###P <0.001 vs control group; ***P <0.001, **P <0.01, *P <0.05 vs model group; (c-d) Effect of

pazopanib on the impairment of spontaneous alteration behavior in the Y-maze test in rats. Results were expressed as mean ± SEM (n=10-12) and analyzed with one-way ANOVA, followed by Dunnett's post test for multiple comparisons. ###P <0.001 vs control group; ***P <0.001, **P <0.01, *P <0.05 vs model group;

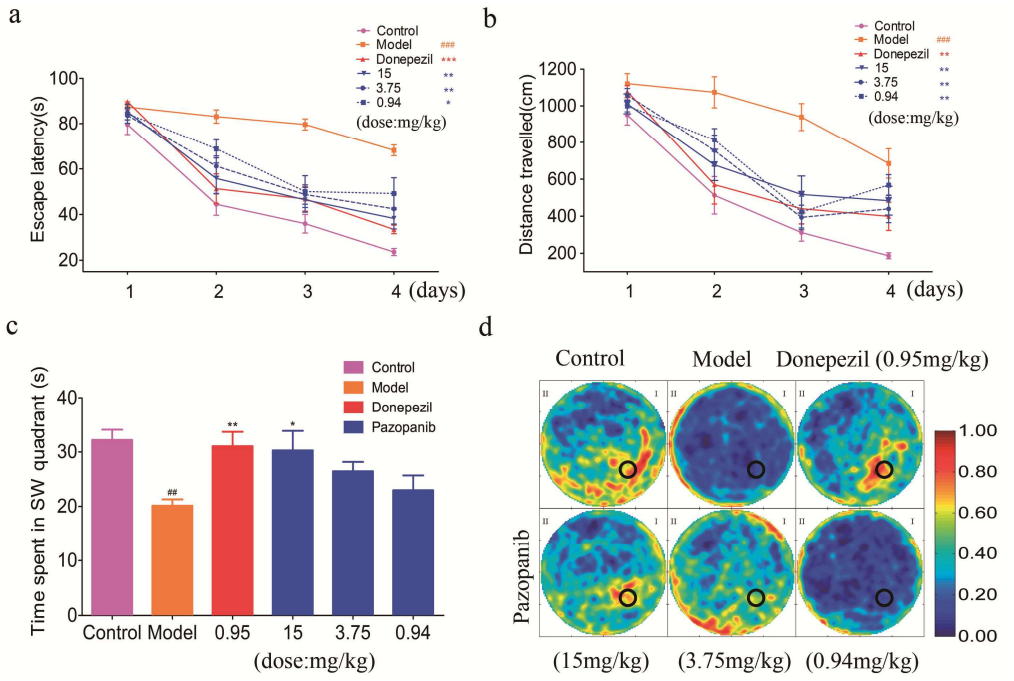

Figure 5. Effect of pazopanib on memory and cognition impairment in the Morris water maze test. (a) Effect of pazopanib on spatial memory impairment in reference memory test of water maze test in rats; (b) Swimming distance to find the safety platform. Results were expressed as mean ± SEM (n=10-12) and analyzed with repeated measures ANOVA followed by Dunnett's post test for multiple comparisons. ###P <0.001 vs control group; ***P <0.001, **P <0.01, *P <0.05 vs model group; (c) Effect of pazopanib on spatial memory impairment in probe test of water maze test in rats. The vertical axis represents the time spent in the fourth quadrant where the

platform was located. Results were expressed as means ± SEM. (n=10-12). ##P <0.01 vs control group; **P <0.01, *P <0.05 vs model group; (d) Spatial preference in probe test of water maze. The heat map is used to represent the frequently visited area by orange and red. The frequency of crossing is calculated as (number of crossing at each point)/(maximum number of crossing at all points). The redness represents the most frequently visited area. The location of the platform is represented in black circle.

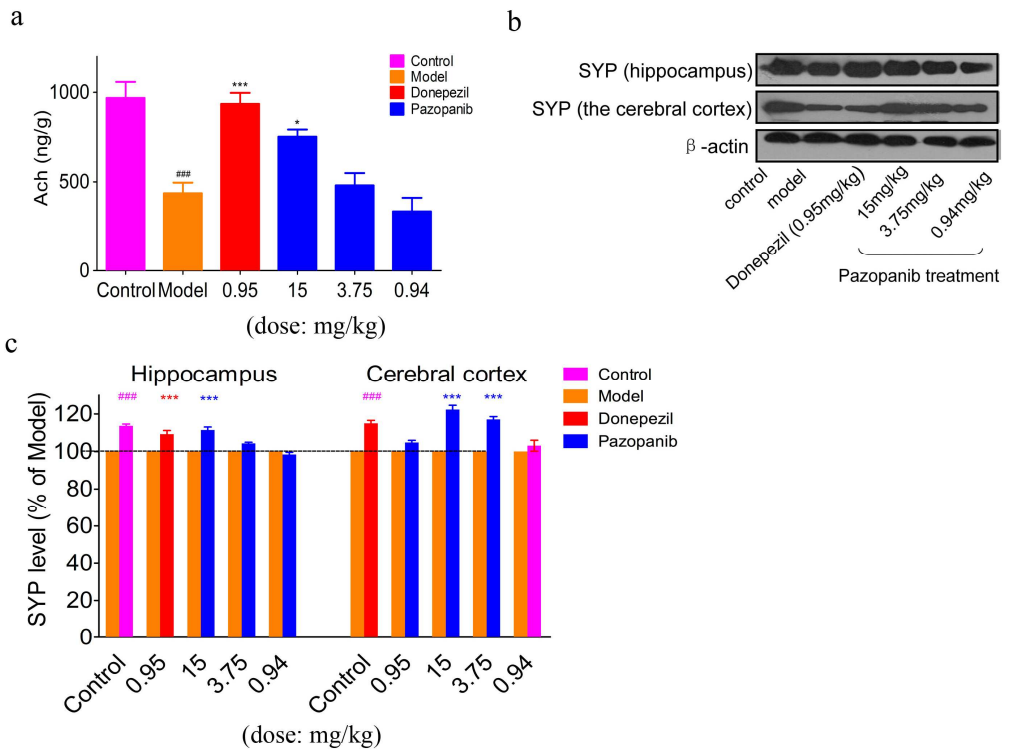

Figure 6. Effect of pazopanib on the hippocampal level of Ach and expression of synaptic marker. (a) The increase of Ach level in hippocampus after the treatment of donepezil and pazopanib in rat model. Results were expressed as mean ± SEM (n=6) and analyzed with one-way ANOVA, followed by Dunnett's post test for multiple comparisons. ###P <0.001 vs. control group; ***P <0.001，*P <0.05 vs. model group;

514 (b-c) Effect of pazopanib on the expression of synapse-related protein SYP in the
515 hippocampus and the cerebral cortex of rat model. The intensity of each protein band
516 was quantified by densitometry using the Quantity One software (Bio-Rad, Hercules,
517 CA, USA), and then corrected with the corresponding β-actin level. Results were
518 expressed as mean ± SEM (n=6) and analyzed with one-way ANOVA, followed by
519 Dunnett's post test for multiple comparisons. ###P <0.001 vs control group; ***P
520 <0.001 vs. model group.
521

References

1. Blennow K, de Leon MJ, & Zetterberg H (2006) Alzheimer's disease. *Lancet* 368(9533):387-403.
2. Lees AJ & Smith E (1983) Cognitive deficits in the early stages of Parkinson's disease. *Brain : a journal of neurology* 106 (Pt 2):257-270.
3. Walker FO (2007) Huntington's Disease. *Seminars in neurology* 27(2):143-150.
4. Ballard C*, et al.* (2011) Alzheimer's disease. *Lancet* 377(9770):1019-1031.
5. Corbett A*, et al.* (2012) Drug repositioning for Alzheimer's disease. *Nature reviews. Drug discovery* 11(11):833-846.
6. Wlodawer A & Erickson JW (1993) Structure-based inhibitors of HIV-1 protease. *Annual review of biochemistry* 62:543-585.
7. Wang J*, et al.* (2007) Quantifying intrinsic specificity: a potential complement to affinity in drug screening. *Physical review letters* 99(19):198101.
8. Yan Z, Zheng X, Wang E, & Wang J (2013) Thermodynamic and kinetic specificities of ligand binding. *Chem. Sci.* 4:2387-2395.
9. Wang J & Verkhivker GM (2003) Energy landscape theory, funnels, specificity, and optimal criterion of biomolecular binding. *Physical review letters* 90(18):188101.
10. Onuchic JN, Luthey-Schulten Z, & Wolynes PG (1997) Theory of protein folding: the energy landscape perspective. *Annual review of physical chemistry* 48:545-600.

11. Liu Z, Zheng X, Yang X, Wang E, & Wang J (2009) Affinity and specificity of levamlodipine-human serum albumin interactions: insights into its carrier function. *Biophysical journal* 96(10):3917-3925.
12. Zheng X, Liu Z, Li D, Wang E, & Wang J (2013) Rational drug design: the search for Ras protein hydrolysis intermediate conformation inhibitors with both affinity and specificity. *Current pharmaceutical design* 19(12):2246-2258.
13. Law V*, et al.* (2014) DrugBank 4.0: shedding new light on drug metabolism. *Nucleic acids research* 42(Database issue):D1091-1097.
14. Muchmore SW, Souers AJ, & Akritopoulou-Zanze I (2006) The use of three-dimensional shape and electrostatic similarity searching in the identification of a melanin-concentrating hormone receptor 1 antagonist. *Chemical biology & drug design* 67(2):174-176.
15. Bostrom J, Grant JA, Fjellstrom O, Thelin A, & Gustafsson D (2013) Potent fibrinolysis inhibitor discovered by shape and electrostatic complementarity to the drug tranexamic acid. *Journal of medicinal chemistry* 56(8):3273-3280.
16. Ma DL, Chan DS, & Leung CH (2013) Drug repositioning by structure-based virtual screening. *Chemical Society reviews* 42(5):2130-2141.
17. Dudley JT, Deshpande T, & Butte AJ (2011) Exploiting drug-disease relationships for computational drug repositioning. *Briefings in bioinformatics* 12(4):303-311.
18. Aubry L*, et al.* (2008) Striatal progenitors derived from human ES cells mature into DARPP32 neurons in vitro and in quinolinic acid-lesioned rats. *Proceedings of the National Academy of Sciences of the United States of America* 105(43):16707-16712.
19. Milletti F & Vulpetti A (2010) Predicting polypharmacology by binding site similarity: from kinases to the protein universe. *Journal of chemical information and modeling* 50(8):1418-1431.
20. Zhang Y & Skolnick J (2005) TM-align: a protein structure alignment algorithm based on the TM-score. *Nucleic acids research* 33(7):2302-2309.
21. Kryger G, Silman I, & Sussman JL (1999) Structure of acetylcholinesterase complexed with E2020 (Aricept): implications for the design of new anti-Alzheimer drugs. *Structure* 7(3):297-307.
22. Karasawa J, Hashimoto K, & Chaki S (2008) D-Serine and a glycine transporter inhibitor improve MK-801-induced cognitive deficits in a novel object recognition test in rats. *Behavioural brain research* 186(1):78-83.
23. Conrad CD, Galea LA, Kuroda Y, & McEwen BS (1996) Chronic stress impairs rat spatial memory on the Y maze, and this effect is blocked by tianeptine pretreatment. *Behavioral neuroscience* 110(6):1321-1334.
24. Morris R (1984) Developments of a water-maze procedure for studying spatial learning in the rat. *Journal of neuroscience methods* 11(1):47-60.

25. Arenas E, Perez-Navarro E, Alberch J, & Marsal J (1993) Selective resistance of tachykinin-responsive cholinergic neurons in the quinolinic acid lesioned neostriatum. *Brain research* 603(2):317-320.
26. Hilbe M, Guscetti F, Wunderlin S, & Ehrensperger F (2005) Synaptophysin: an immunohistochemical marker for animal dysautonomias. *Journal of comparative pathology* 132(2-3):223-227.
27. Sze CI*, et al.* (1997) Loss of the presynaptic vesicle protein synaptophysin in hippocampus correlates with cognitive decline in Alzheimer disease. *Journal of neuropathology and experimental neurology* 56(8):933-944.
28. King DL & Arendash GW (2002) Maintained synaptophysin immunoreactivity in Tg2576 transgenic mice during aging: correlations with cognitive impairment. *Brain research* 926(1-2):58-68.
29. Chen X*, et al.* (2011) PSD-95 is required to sustain the molecular organization of the postsynaptic density. *The Journal of neuroscience : the official journal of the Society for Neuroscience* 31(17):6329-6338.
30. Dudley JT*, et al.* (2011) Computational repositioning of the anticonvulsant topiramate for inflammatory bowel disease. *Science translational medicine* 3(96):96ra76.
31. Fan R*, et al.* (2007) Minocycline reduces microglial activation and improves behavioral deficits in a transgenic model of cerebral microvascular amyloid. *The Journal of neuroscience : the official journal of the Society for Neuroscience* 27(12):3057-3063.
32. Cramer PE*, et al.* (2012) ApoE-directed therapeutics rapidly clear beta-amyloid and reverse deficits in AD mouse models. *Science* 335(6075):1503-1506.
33. Yan Z & Wang J (2012) Specificity quantification of biomolecular recognition and its implication for drug discovery. *Scientific reports* 2:309.
34. Yan Z & Wang J (2013) Optimizing scoring function of protein-nucleic acid interactions with both affinity and specificity. *PloS one* 8(9):e74443.
35. Naylor E*, et al.* (2009) Identification of a chemical probe for NAADP by virtual screening. *Nature chemical biology* 5(4):220-226.
36. Xie L & Bourne PE (2011) Structure-based systems biology for analyzing off-target binding. *Current opinion in structural biology* 21(2):189-199.
37. Xie L, Evangelidis T, & Bourne PE (2011) Drug discovery using chemical systems biology: weak inhibition of multiple kinases may contribute to the anti-cancer effect of nelfinavir. *PLoS computational biology* 7(4):e1002037.
38. Kinnings SL*, et al.* (2009) Drug discovery using chemical systems biology: repositioning the safe medicine Comtan to treat multi-drug and extensively drug resistant tuberculosis. *PLoS computational biology* 5(7):e1000423.
39. Zivi A, Cerbone L, Recine F, & Sternberg CN (2012) Safety and tolerability of pazopanib in the treatment of renal cell carcinoma. *Expert opinion on drug safety* 11(5):851-859.

40. Scali C*, et al.* (2003) The selective cyclooxygenase-2 inhibitor rofecoxib suppresses brain inflammation and protects cholinergic neurons from excitotoxic degeneration in vivo. *Neuroscience* 117(4):909-919.
41. Portera-Cailliau C, Hedreen JC, Price DL, & Koliatsos VE (1995) Evidence for apoptotic cell death in Huntington disease and excitotoxic animal models. *The Journal of neuroscience : the official journal of the Society for Neuroscience* 15(5 Pt 2):3775-3787.
42. Leaver KR*, et al.* (2012) Effects of translocator protein (18 kDa) ligands on microglial activation and neuronal death in the quinolinic-acid-injected rat striatum. *ACS chemical neuroscience* 3(2):114-119.
43. Beal MF, Ferrante RJ, Swartz KJ, & Kowall NW (1991) Chronic quinolinic acid lesions in rats closely resemble Huntington's disease. *The Journal of neuroscience : the official journal of the Society for Neuroscience* 11(6):1649-1659.
44. Li C, Ebrahimi A, & Schluesener H (2013) Drug pipeline in neurodegeneration based on transgenic mice models of Alzheimer's disease. *Ageing research reviews* 12(1):116-140.